Journal of Thermal Analysis and Calorimetry (2020) 139:2155–2163
https://doi.org/10.1007/s10973-019-08614-w

Thermal stability assessment of 4-amino-1,2,4-triazole picrate using thermal analysis method

Bin Zhang[1] · Shang-Hao Liu[2]

Received: 9 April 2019 / Accepted: 19 July 2019 / Published online: 1 August 2019

Abstract

4-Amino-1,2,4-triazole picrate (4-ATPA) is synthesized to reduce the corrosiveness of picric acid (PA) to metals, which simultaneously maintains the detonation performance of PA and the advantages of 4-amino-1,2,4-triazole. In this work, the thermal stability of 4-ATPA is estimated using thermogravimetric analysis (TG) and accelerating rate calorimeter. The dynamic TG experimental results suggest that the onset temperature is at the range of 189.0–220.0 °C under different heating rates. The average apparent activation energy of 4-ATPA is 112.0 ± 1.1 kJ mol^{-1} using Flynn–Wall–Ozawa, Starink, and Kissinger methods based on the multiple heating rates. The isothermal TG experiments indicate that 4-ATPA will be decomposed 10.0% within 1 day if the temperature exceeded 150.7 °C and will be decomposed 10.0% within 10.0 h if the temperature exceeded 162.6 °C. The adiabatic tests depicted that the exothermic reaction initiates at 186.0 °C and a rises sharply at 306.7 °C with the maximum self-heating rate of 4775.5 °C min^{-1}. The exothermic event is accompanied by a pressure rise of 39.7 bar, which confirms the vulnerability of 4-ATPA to undergo catastrophic explosion.

Keywords 4-Amino-1,2,4-triazole picrate · Thermal stability · Thermogravimetric analysis · Accelerating rate calorimeter · Exothermic reaction

List of symbols

A	Pre-exponential factor (min^{-1})
C_{pb}	Heat capacity of test bomb (J g^{-1} K^{-1})
C_{ps}	Heat capacity of sample (J g^{-1} K^{-1})
E_a	Apparent activation energy (kJ mol^{-1})
h	Planck constant (6.626 × 10^{-34} J s)
k	Arrhenius rate constant (min^{-1})
k_B	Boltzmann constant (1.3807 × 10^{-27} J K^{-1})
M_b	Mass of test bomb (g)
M_s	Mass of sample (g)
m_m	Measured maximum self-heating rate (°C min^{-1})
$m_{m,s}$	Corrected maximum self-heating rate (°C min^{-1})
P_{max}	Maximum pressure (bar)
p_m	Maximum pressure rise rate (bar min^{-1})
R	Universal gas constant (8.314 J mol^{-1} K^{-1})
r	Linear correlation coefficient (Dimensionless)
T	Reaction temperature (°C)
T_{end}	Termination decomposition temperature (°C)
T_{max}	Maximum temperature (°C)
TMR_{ad}	Measured time to maximum rate under adiabatic condition (min)
$TMR_{ad,s}$	Measured time to maximum rate under adiabatic condition (min)
T_{onset}	Onset decomposition temperature (°C)
T_p	Peak temperature (°C)
T_{p0}	Peak temperature when heating rate closed to zero (°C)
T_{start}	Start decomposition temperature (°C)
$T_{z/y}$	Temperature of decomposition z at a time y (°C)
$T_{0.1}$	Temperature of decomposition 10.0% (°C)
$T_{0.1/y}$	Temperature of decomposition 10.0% in y h (°C)
$T_{0.1/10h}$	Temperature of decomposition 10.0% in 10.0 h (°C)
$\Delta G^{\neq}$	Gibbs free energy (kJ mol^{-1})
$\Delta H^{\neq}$	Enthalpy (kJ mol^{-1})
$\Delta S^{\neq}$	Entropy (J mol K^{-1})

✉ Shang-Hao Liu
shliu998@163.com

[1] School of Chemical Engineering, Anhui University of Science and Technology (AUST), Huainan 232001, Anhui, China

[2] State Key Laboratory of Mining Response and Disaster Prevention and Control in Deep Coal Mines, AUST, Huainan 232001, Anhui, China

ΔT_{ad}	Measured adiabatic temperature rise (°C)
$\Delta T_{ad,s}$	Corrected adiabatic temperature rise (°C)
α	Degree of conversion (dimensionless)
β	Heating rate (°C min^{-1})
Φ	Thermal inertia (dimensionless)

Introduction

Picric acid (PA), one of the significant nitroaromatic derivatives, is widely used in antiseptic, burn treatment, and dyes industries [1–5]. However, PA is not an eco-friendly substance, which cannot be biodegraded. Moreover, due to the formidable irritant of PA, long-term exposure will cause diarrhea, nausea, vomiting, diarrhea, and other symptoms [6–8]. Based on the low sensitivity and higher energy than 2, 4, 6-trinitrotoluene, PA is also used as energetic material [1, 9–11]. Seriously, PA can easily form metal picrate salts, which are more sensitive and hazardous than the acid itself [4, 12]. Therefore, PA needs to be modified to improve security during production, storage, and use.

4-Amino-1,2,4-triazole (ATR) is one type of high nitrogen heterocyclic compounds, which combines the negligible vapor pressure, low melting point, and wide electrochemical windows of ionic liquids (ILs) [13–15]. Meanwhile, ATR has other particular properties, such as high nitrogen content, high positive enthalpy of formation, and dense structure [16–18]. Due to the coordinated amino nitrogen and heterocyclic nitrogen, ATR can form as a coordinating compound. Therefore, based on the weakly alkaline nature, ATR reacts with PA forming energetic ionic compound 4-amino-1,2,4-triazole picrate (4-ATPA), which solves the puzzle of large acidity of PA and maintains the high nitrogen content and low sensitivity of ATR [19].

The synthetic route of 4-ATPA is shown in Fig. 1 [16]. The crystal structure was fully studied since be synthesized. Jin et al. confirmed the structure of 4-ATPA by single-crystal X-ray and NMR [16]. However, the thermal stability of 4-ATPA has not been evaluated, which refers to the potential hazards of the production, storage, transportation and use through actual measurement and calculation. The use of reasonable methods for evaluating the thermal stability of energetic materials has significant meaning. Among the various evaluation methods, the basic thermal stability test evaluation method (including thermogravimetric analysis (TG), differential scanning calorimetry (DSC), and differential thermal analysis (DTA)), which has the advantages of little sample volume, brief test period and high security, is the representative evaluation pattern. In this paper, we apply this method to evaluate the thermal stability of 4-ATPA. The main steps are shown as follows:

1. To obtain the thermal decomposition characteristics of 4-ATPA, TG is employed under non-isothermal and isothermal conditions, respectively.
2. To calculate the thermokinetic parameters, such as the apparent activation energy (E_a) and the pre-exponential factor (A), Flynn–Wall–Ozawa (FWO), Starink, and Kissinger methods are adopted.
3. To estimate the process safety parameters in the case of energy accumulation, accelerating rate calorimeter (ARC) is used to simulate the thermal runaway reaction.

Experimental and methods

Materials

Ninety-eight mass% 4-ATPA, which in the form of yellow powder, is purchased from Hua Wei Rui Ke Chemical Co., Beijing, China. Before experiments, the sample is dried under vacuum at 40.0 °C for 48 h for reducing the impact of impurity water.

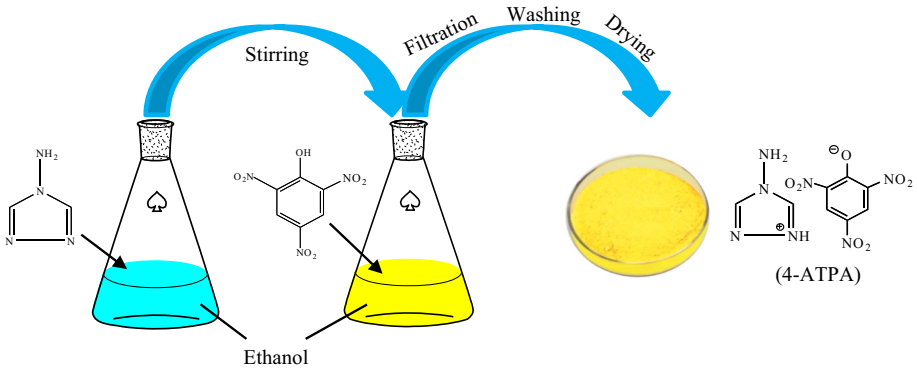

Fig. 1 Synthesis route of 4-ATPA

Analytical methods

TG experiments are performed by STA7200RV (Hitachi Instruments, Inc., Tokyo, Japan). The open alumina crucible is adopted, which is loaded ca. 3.0 mg sample for each experiment. Both non-isothermal and isothermal experiments are under nitrogen atmosphere with a gas flow in 200.0 mL min^{-1}. The short-term thermal stability of 4-ATPA was evaluated in the range of 30.0–500.0 °C with the heating rates of 1.0, 2.0, 4.0, and 8.0 °C min^{-1}. Moreover, the isothermal experiments are accomplished at 150.0–200.0 °C with the end criterion of 10.0% mass loss.

The simulation of the thermal runaway reaction of 4-ATPA is demonstrated by ES-ARC (Thermal Hazard Technology, Inc., Bletchley, England). The adopted Ti-LCQ test bomb (Thermal Hazard Technology, Inc.) has a 9.5 mL volume, which is loaded 300 ± 10 mg sample for each test. The standard heat-wait-search (H-W-S) mode is applied based on the ASTM E1981-98(2012)e2 [20]. The experiment is started at 160.0 °C and ended at 400.0 °C. The system temperature is raised 3.0 °C for each step and the adiabatic state kept at wait time. Then the system is allowed enter into search mode with a threshold self-heating value of 0.2 °C min^{-1} after a 15.0 min as wait time.

Theoretical calculation

According to the recommendations of International Confederation for Thermal Analysis and Calorimetry (ICTAC) Kinetic Committee [21, 22], three isoconversional methods (FWO, Starink, and Kissinger methods) are applied to calculate the thermokinetic parameters.

In general, the thermal degradation of 4-ATPA is complied with Eq. (1), which is shown as follows [23, 24]:

$$\frac{d\alpha}{dt} = k(T) \times f(\alpha) \tag{1}$$

where $d\alpha/dt$ represents the conversion rate, $k(T)$ is the Arrhenius rate constant, and $f(\alpha)$ is the differential mechanism function.

Considering the impact of heating rate, Eq. (1) can be rearranged to Eq. (2) based on the Arrhenius equation, which is expressed as [23, 24]:

$$\frac{d\alpha}{dT} = \frac{A}{\beta} \times \exp\left(-\frac{E_a}{RT}\right) \times f(\alpha) \tag{2}$$

where A is the pre-exponential factor, β is the heating rate, E_a is the apparent activation energy, and R is the universal gas constant (8.314 J mol^{-1} K^{-1}).

FWO method is a typical isoconversional method, which is through diverse heating rate curves to determine the thermokinetic parameters. The FWO formula is expressed as [25, 26]:

$$\lg(\beta) = \lg\left[\frac{AE_a}{RG(\alpha)}\right] - 2.315 - 0.4567\frac{E_a}{RT} \tag{3}$$

where $G(\alpha)$ is the integral mechanism function. Plotting $1/T$ versus $\lg(\beta)$ can form a straight line, and E_a is obtained from the slope.

Starink method also demands multiple heating rates to determine the thermokinetic parameters, which is shown as follows [27]:

$$\ln\frac{\beta}{T^{1.8}} = C_s - \frac{E_a}{RT} \tag{4}$$

where C_s is constant. E_a is obtained by plotting $1/T$ versus $\ln(\beta\ T^{-1.8})$.

Kissinger method can be expressed as Eq. (5) [28]:

$$\ln\frac{\beta}{T_p^2} = \ln\frac{AR}{E_a} - \frac{E_a}{RT_p} \tag{5}$$

where T_p is peak temperature. Therefore, E_a and A can be obtained from the slope and intercept, respectively.

The thermodynamic parameters of 4-ATPA such as entropy ($\Delta S^{\neq}$), enthalpy ($\Delta H^{\neq}$) and Gibbs free energy ($\Delta G^{\neq}$) are also determined based on the results of the Kissinger method. The relationship between A and $\Delta S^{\neq}$ can be expressed by Eq. (6), which is expressed as:

$$A = \frac{k_B T_{p0}}{h}\exp\left(\frac{\Delta S^{\neq}}{R}\right) \tag{6}$$

where k_B is the Boltzmann constant (1.3807×10^{-27} J K^{-1}), h represents the Planck constant (6.626×10^{-34} J s), and T_{p0} is peak temperature when the heating rate closes to 0, which can be determined by Eq. (7), as shown follows [29]:

$$T_{pi} = a + b\beta_i + c\beta_i^2 + d\beta_i^3 \tag{7}$$

where a, b, c, and d are coefficients. The values of the four coefficients can be calculated using four groups of heating rate β_i and T_p. When $\beta \to 0$, the value of T_p is defined as T_{p0}, which is equal to the value of coefficient a.

Then the $\Delta H^{\neq}$ and $\Delta G^{\neq}$ can be calculated using Eqs. (8) and (9) once $\Delta S^{\neq}$ is obtained [26].

$$\Delta H^{\neq} = E_a - RT_{p0} \tag{8}$$

$$\Delta G^{\neq} = \Delta H^{\neq} - T_{p0}\Delta S^{\neq} \tag{9}$$

Results and discussion

Thermal decomposition process

The short-term thermal stability of 4-ATPA is evaluated by dynamic experiments. As shown in Fig. 2, the multiple

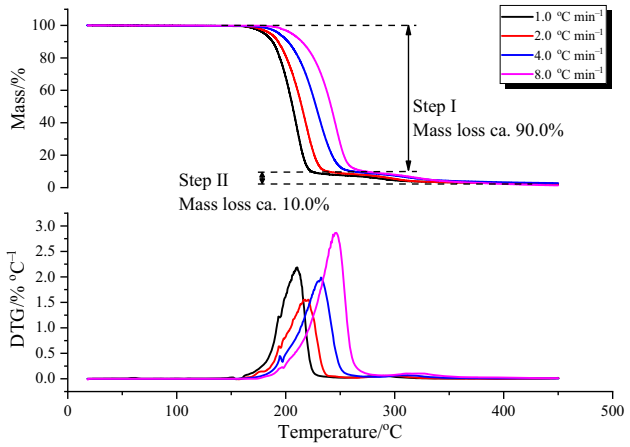

Fig. 2 TG-DTG curves of 4-ATPA

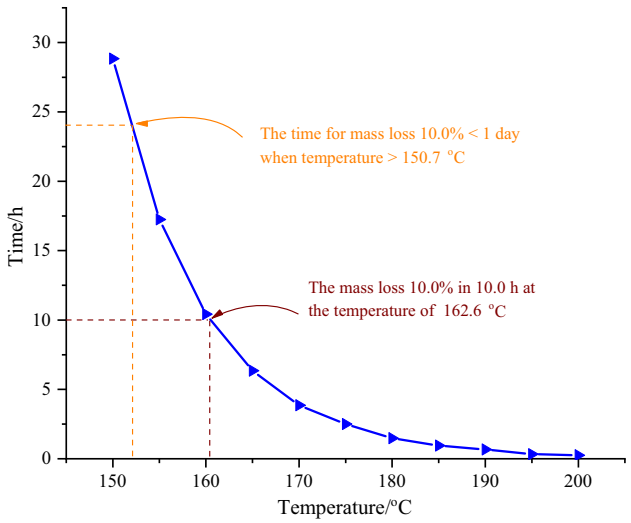

Fig. 3 The relationship between the time and temperature for decomposing 10.0% under isothermal conditions of 4-ATPA

heating rate curves of 4-ATPA under nitrogen atmosphere are obtained. The decomposition reactions undergo two stages. Step I is the main thermal decomposition stage, which has approximately 90.0% mass loss. Step II is the end of the thermal decomposition with ca. 10.0% mass loss.

Generally, the short-term thermal stability is described by the onset temperature (T_{onset}), which is obtained from the intersection of the baseline mass and the tangent of the mass dependence on the temperature curve as decomposition occurs [30, 31]. As shown in Table 1, T_{onset} of 4-ATPA under different heating rates is at the range of 189.0–220.0 °C. However, the actual thermal decomposition starts at a lower temperature (T_{start}): T_{start} is approximately 30.0–35.0 °C lower than T_{onset}. The results indicate that T_{onset} overestimates the thermal stability since the actual critical thermal temperature is passed through quickly. The peak temperature (T_p) is another parameter to character the short-term thermal stability. Obviously, the peak temperature for stage I (T_{p1}) is at the range of 210.0–250.0 °C, which is ca. 80.0 °C lower than the peak temperature for stage II (T_{p2}). $T_{0.1}$ (the temperature at which a mass loss of 10.0% is observed) also is adopted to determine the short-term thermal stability. As revealed in Table 1, the values of $T_{0.1}$ and T_{onset} are almost the same. Compared with T_{onset}, $T_{0.1}$ is a parameter with practical physical significance. However, both T_{onset} and $T_{0.1}$ merely represent the short-term thermal stability of 4-ATPA.

Long-term thermal stability assessment

The isothermal experiments are determined to overcome the limitations of dynamic TG method and to obtain more profound parameters for estimating the thermal stability. To interpret the long-term thermal stability, the right criterion is to be adopted, and another parameter $T_{z/y}$ (which denotes the degree of thermal decomposition z at a time y) is proposed [30]. In this work, we apply $T_{0.1/y}$ to assess the long-term thermal stability of 4-ATPA.

Figure 3 show the relationship between the isothermal time and selected temperature for decomposing 10.0% of 4-ATPA. Obviously, as the temperature increases, the time required for 4-ATPA to decompose 10.0% is rapidly decreased. According to the simulation curve, 4-ATPA will decompose 10.0% within 1 day if the temperature exceeds 151.0 °C. $T_{0.1/10h}$ is a more common and accurate parameter for evaluating the long-term thermal stability [31, 32]. The $T_{0.1/10h}$ value of 4-ATPA is ca. 163.0 °C, which is significantly lower than the value of T_{onset}. The results mean that the maximum operating temperature of 4-ATPA should be reduced to 160.0 °C due to safety concerns.

Table 1 Characteristic temperatures of 4-ATPA

β/°C min^{-1}	T_{start}/°C	T_{onset}/°C	T_{p1}/°C	T_{p2}/°C	T_{end}/°C	$T_{0.1}$/°C
1.0	162	189	210	290	316	188
2.0	166	196	219	303	322	194
4.0	171	206	232	312	335	202
8.0	183	220	246	320	348	215

Kinetics of thermal decomposition

Generally, the conversions at the range of 0.1–0.9 are applied for calculation, since the conversion at the initial and termination stages of thermal degradation is significantly impacted by the selected baseline and the noise of the system [33–35]. As can be seen in Fig. 4, lg(β) for KAS method and ln($\beta\ T^{-1.8}$) for Starink method are plotted against ($10^3\ T^{-1}$) and ln($\beta\ T_p^{-2}$) for Kissinger method is plotted against ($10^3\ T_p^{-1}$) to determine E_a, respectively. The superior linear correlation with $r > 0.98$ is obtained in all the cases. The E_a values that are determined from the slopes of the fitting equations for each conversion are presented in Fig. 5.

As can be seen, the E_a value of 4-ATPA is mainly degressive within the mentioned conversions range both for FWO and Starink methods. Vyazovkin et al. have demonstrated that the process can be considered as a single-step model if the fluctuation range of E_a is minor and no shoulders appeared in the reaction rate curve [21]. Obviously, the decomposition of 4-ATPA is a complex reaction, which cannot be regarded as a single-step kinetic model since the E_a value is dependent on conversion.

Table 2 lists the thermokinetic parameters of 4-ATPA obtained by different methods. The average E_a is 112.4 ± 1.2, 110.7 ± 1.0, and 113.0 ± 1.1 kJ mol^{-1} obtained by FWO, Starink, and Kissinger methods, respectively, which have little differences between the three methods. Based on Eq. (5), the determined ln(A) is 25.3 ± 0.2 min^{-1}.

The $\Delta S^{\neq}$, $\Delta H^{\neq}$, and $\Delta G^{\neq}$ resolved by Eqs. (6)–(9) are 38.2 J mol K^{-1}, 109.0 kJ mol^{-1}, and 91 kJ mol^{-1}, respectively. Obviously, the value of $\Delta G^{\neq}$ is much larger than 0, which indicates the thermal decomposition reaction of 4-ATPA will be initiated until adequate energy is provided.

Adiabatic test and analysis

From the adiabatic test, the key parameters for quantizing the runaway reaction of the energetic materials (such as onset temperature, self-heating rate, and pressure data) can be obtained. Figure 6 exhibits the variations of temperature and pressure during the process. As can be seen, the decomposition reaction of 4-ATPA under the adiabatic condition is quite violent. The exothermic reaction commences at 186.0 °C with an initial self-heating rate of 0.22 °C min^{-1}. The runaway reaction ends up at 322.2 °C after 87.3 min, and the adiabatic temperature increases (ΔT_{ad}) is 136.2 °C. Meanwhile, the pressure increased to 38.4 bar throughout the entire exothermic process and the final pressure reaches 39.7 bar. However, deviations exist

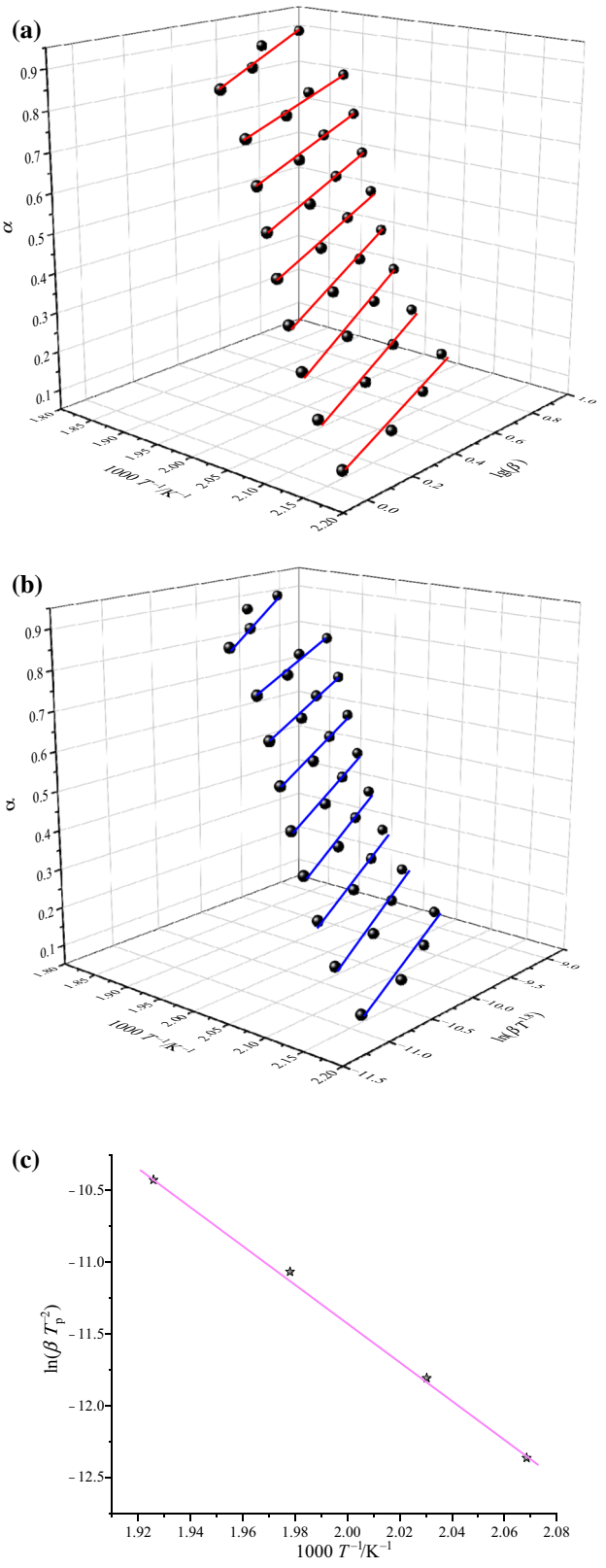

Fig. 4 Liner curves obtained by **a** FWO method, **b** Starink method, and **c** Kissinger method

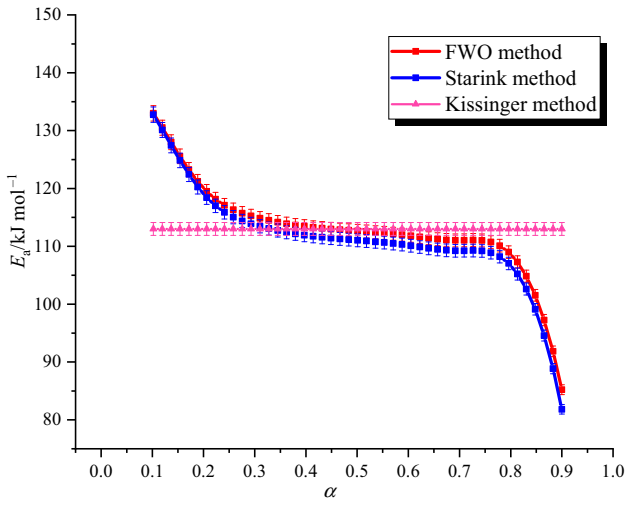

Fig. 5 E_a for thermal decomposition of 4-ATPA dependent on α

Table 2 Thermokinetic parameters obtained from various methods of 4-ATPA

Method	E_a/kJ mol^{-1}	A/min^{-1}	r
FWO	112.4 ± 1.2	–	0.9851
Starink	110.7 ± 1.0	–	0.9880
Kissinger	113.0 ± 1.1	(1.01 ± 0.2) × 10^{11}	0.9946

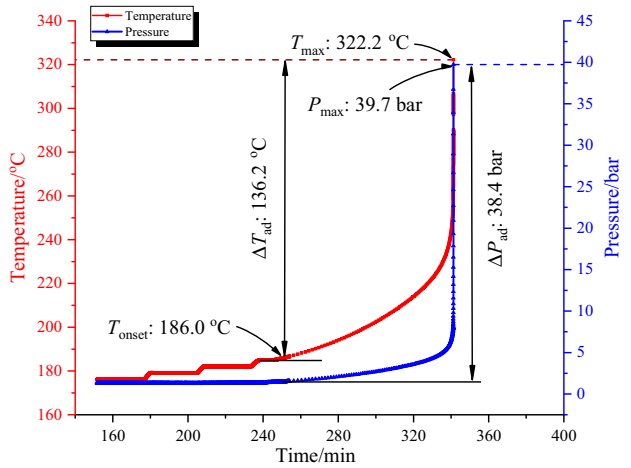

Fig. 6 Temperature and pressure versus time for the thermal decomposition of 4-ATPA by ARC

in these values because some heat is absorbed by the test bomb during the exothermic reaction; thus, the experimental data needs to be amended.

The variation of pressure versus temperature is presented in Fig. 7, indicating that the exothermic reaction system pressure has two significantly different change tendency stages: Stage I ($T < 259.1$ °C) and stage II ($T > 259.1$ °C). In stage I, the pressure increases slowly, which may be caused by two reasons: The air pressure

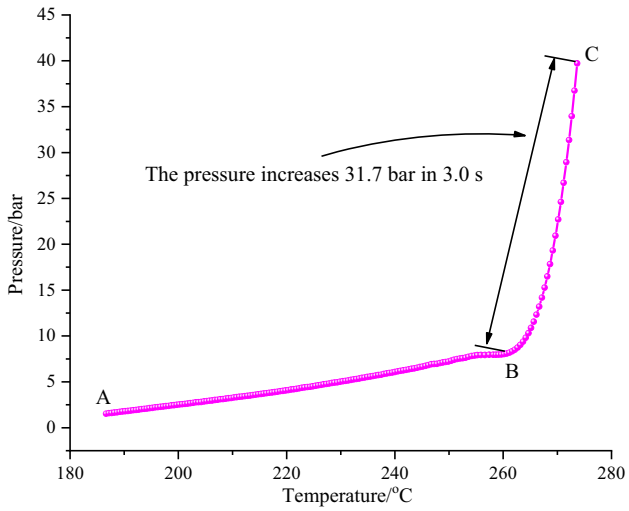

Fig. 7 Pressure versus temperature under adiabatic condition of 4-ATPA by ARC

increases slowly with the temperature increase; the other one is that 4-ATPA decomposes to produce little gas products. In stage II, the pressure increases sharply, which is raised to 31.7 bar within 3.0 s. This phenomenon may be owing to the fierce decomposition of 4-ATPA and produces a large amount of gas products.

Figure 8 reveals the variation of self-heating rate and pressure rise rate versus temperature. Obviously, the self-heating rate reaches the maximum value of 4775.5 °C min^{-1} within 87.2 min. The pressure rise rate rises slowly from the initial of 0.019 to 6.7 bar min^{-1} in stage I. Then the pressure rise rate increases rapidly to the maximum value of 1491.7 bar min^{-1}. The results indicate the thermal decomposition reaction of 4-ATPA under adiabatic conditions is vigorous and may result in a great disaster.

Data correction

The heat produced from the exothermic reaction of energetic materials is used to heat the material, the test bomb, and surroundings. The scale of energy that is used to heat the test bomb is defined as thermal inertia (Φ), which is expressed as follows [36]:

$$\Phi = \frac{M_s C_{ps} + M_b C_{pb}}{M_s C_{ps}} \tag{10}$$

where M_s is the mass of the sample, C_{ps} is the heat capacity of the sample, M_b is the mass of the test bomb, and C_{pb} is the heat capacity of the test bomb. Hence, the test parameters need to be corrected using Φ.

The corrected methods are shown as follows [37]:

$$\Delta T_{ad,s} = \Phi \Delta T_{ad} \tag{11}$$

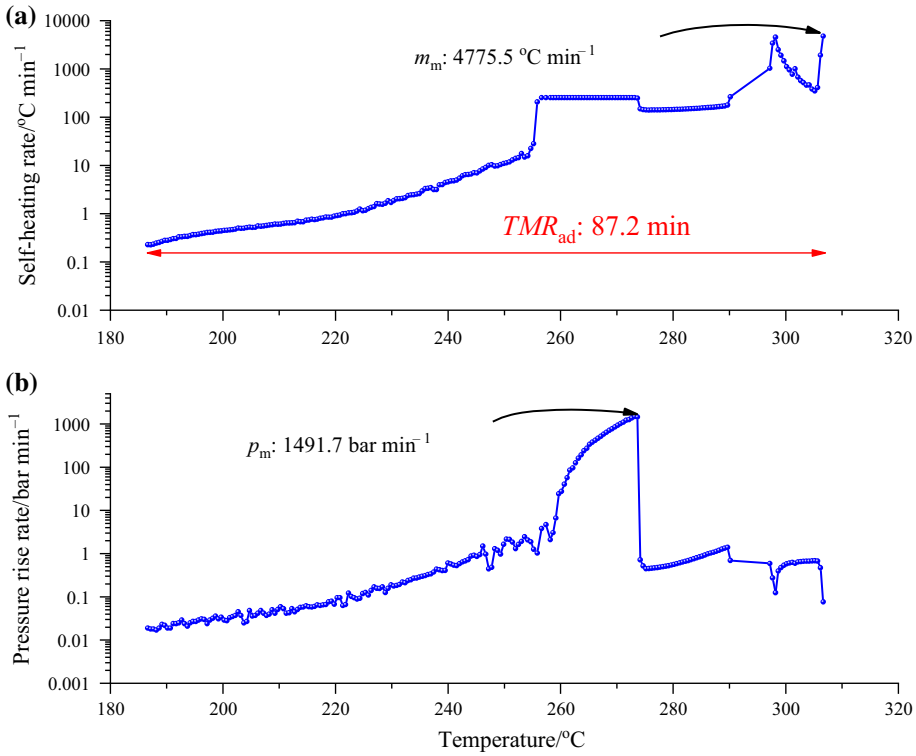

Fig. 8 **a** Self-heating rate and **b** pressure rise rate versus temperature of 4-ATPA by ARC

$$m_{m,s} = \Phi m_m \quad (12)$$

$$\mathrm{TMR}_{ad,s} = \frac{\mathrm{TMR}_{ad}}{\Phi} \quad (13)$$

where $\Delta T_{ad,s}$ is the corrected adiabatic temperature rise, ΔT_{ad} is the measured adiabatic temperature rise, $m_{m,s}$ is the corrected maximum self-heating rate, m_m is the measured maximum self-heating rate, $\mathrm{TMR}_{ad,s}$ is the corrected time to maximum rate, TMR_{ad} is the measured time to maximum rate.

The corrected data are listed in Table 3, indicating that Φ has significant impact on the tested temperature parameters: The measured adiabatic temperature rise and maximum self-heating rate are 136.2 °C and 4775.5 °C min^{-1} and after being corrected are 1171.3 °C and 41,069.3 °C min^{-1}. Meanwhile, the time to maximum temperature rise rate decreased from 87.2 to 10.1 min, which indicates that the thermal decomposition of 4-ATPA will occur at a shorter time in the real case of energy accumulation.

Table 3 Measured and corrected thermal decomposition parameters under adiabatic conditions

Parameter	Measured data	Corrected data
Φ	8.6	–
ΔT_{ad}/°C	136.2	1171.3
m_m/°C min^{-1}	4775.5	41,069.3
TMR_{ad}/min	87.2	10.1

Conclusions

In this work, the thermal stability of 4-ATPA is carried out by TG and ARC. The data from dynamic TG experiments suggested that the onset decomposition temperature is at the range of 189.0–220.0 °C under different heating rates and the experimental curves are moved to the high-temperature zone with the increase in heating rate. However, the mass loss is found at the temperature lower than the onset decomposition temperature; thus, the isothermal experiments are applied to assess the long-term thermal stability. The results indicate that 4-ATPA will be decomposed 10.0% within 1 day at ca. 150.7 °C. The average apparent activation energy obtained by three different methods for decomposition process is 112.0 ± 1.1 kJ mol^{-1}.

The adiabatic tests suggested that the initial exothermic temperature of 4-ATPA is 186.0 °C. The endpoint of the violent decomposition reaction is at 322.2 °C within a total time span of 87.3 min. The runaway reaction attained a maximum self-heating rate of 4775.5 °C min^{-1}. Meanwhile, the entire process is accompanied by a pressure rise of 39.7 bar. Considering the heat loss of the experimental

process, the adiabatic temperature rise, maximum self-heating rate, and the time to maximum temperature rise rate are corrected to 1171.3 °C, 41,069.3 °C min^{-1}, and 10.1 min.

Acknowledgments The authors are grateful to the financial support from Anhui Provincial Natural Science Foundation, China, under the Contract Number 1908085ME125.

References

1. Aggarwal P, Misra K, Kapoor S, Bhalla A, Bansal R. Effect of surface oxygen complexes of activated carbon on the adsorption of 2, 4, 6-trinitrophenol. Defence Sci J. 1998;48(2):219–22.
2. Ismail M, Khan MI, Khan SB, Akhtar K, Khan MA, Asiri AM. Catalytic reduction of picric acid, nitrophenols and organic azo dyes via green synthesized plant supported Ag nanoparticles. J Mol Liq. 2018;268:87–101.
3. Dixon DJ, Pando Morejón O. 8.13 Recent developments in the reduction of nitro and nitroso compounds. In: Knochel P editor. Comprehensive organic synthesis II, 2nd edition. Amsterdam: Elsevier; 2014;479–92.
4. Gad SC. Picric Acid. In: Wexler P, editor. Encyclopedia of toxicology. 3rd ed. Oxford: Academic Press; 2014. p. 952–4.
5. Wang H, Chen C, Liu Y, Wu Y, Yuan Y, Zhou Q. A highly sensitive and selective chemosensor for 2, 4, 6-trinitrophenol based on L-cysteine-coated cadmium sulfide quantum dots. Talanta. 2019;198:242–8.
6. Sun X, Wang Y, Lei Y. Fluorescence based explosive detection: from mechanisms to sensory materials. Chem Soc Rev. 2015;44(22):8019–61.
7. Wu YC, Luo SH, Cao L, Jiang K, Wang LY, Xie JC, Wang ZY. Self-assembled structures of N-alkylated bisbenzimidazolyl naphthalene in aqueous media for highly sensitive detection of picric acid. Anal Chim Acta. 2017;976:74–83.
8. Santra DC, Bera MK, Sukul PK, Malik S. Charge-transfer-induced fluorescence quenching of anthracene derivatives and selective detection of picric acid. Chem Eur J. 2016;22(6):2012–9.
9. Rong M, Lin L, Song X, Zhao T, Zhong Y, Yan J, Wang Y, Chen X. A label-free fluorescence sensing approach for selective and sensitive detection of 2,4,6-trinitrophenol (TNP) in aqueous solution using graphitic carbon nitride nanosheets. Anal Chem. 2015;87(2):1288–96.
10. Rajput JK. "ON-OFF" novel fluorescent chemosensors based on nanoaggregates of triaryl imidazoles for superselective detection of nitro-explosive trinitrophenol in multiple solvent systems. Sens Actuators B Chem. 2018;259:990–1005.
11. Kong W, Zhao X, Zhu Q, Gao L, Cui H. Highly chemiluminescent magnetic beads for label-free sensing of 2, 4, 6-trinitrotoluene. Anal Chem. 2017;89:7145–51.
12. Matsukawa M, Matsunaga T, Yoshida M, Fujiwara S. Synthesis and properties of lead picrates. Sci Technol Energ Mater. 2004;65(1):7–13.
13. Süleymanoğlu N, Ünver Y, Ustabaş R, Direkel Ş, Alpaslan G. Antileishmanial activity study and theoretical calculations for 4-amino-1,2,4-triazole derivatives. J Mol Struct. 2017;1144:80–6.
14. Drake G, Hawkins T, Brand A, Hall L, Mckay M, Vij A. Ismail I Energetic, low-melting salts of simple heterocycles. Propellants, Explos, Pyrotech. 2003;28(4):174–80.
15. Xue H, Twamley B, Shreeve JM. Energetic quaternary salts containing Bi(1, 2, 4-triazoles). Inorg Chem. 2005;44(20):7009–13.
16. Jin CM, Ye C, Piekarski C, Twamley B, Shreeve JM. Mono and bridged azolium picrates as energetic salts. Eur J Inorg Chem. 2005;2005(18):3760–7.
17. Chowdhury A, Thynell ST. Confined rapid thermolysis/FTIR/ToF studies of triazolium-based energetic ionic liquids. Thermochim Acta. 2009;485(1):1–13.
18. Chavez DE, Hiskey MA, Gilardi RD. Novel high-nitrogen materials based on nitroguanyl-substituted tetrazines. Org Lett. 2004;6:2889–91.
19. Zorn DD, Boatz J, Gordon MS. Electronic structure studies of tetrazolium-based ionic liquids. J Phys Chem B. 2006;110(23):11110–9.
20. ASTM E1981-98(2012)e2, Standard guide for assessing thermal stability of materials by methods of accelerating rate calorimetry. 2012.
21. Vyazovkin S, Burnham AK, Criado JM, Pérez-Maqueda LA, Popescu C, Sbirrazzuoli N. ICTAC kinetics committee recommendations for performing kinetic computations on thermal analysis data. Thermochim Acta. 2011;520:1–19.
22. Vyazovkin S, Chrissafis K, Lorenzo MLD, Koga N, Pijolat M, Roduit B, Sbirrazzuoli N, Suñol JJ. ICTAC kinetics committee recommendations for collecting experimental thermal analysis data for kinetic computations. Thermochim Acta. 2014;590:1–23.
23. Grigiante M, Brighenti M, Antolini D. Analysis of the impact of TG data sets on activation energy (E_a). J Therm Anal Calorim. 2017;129:553–65.
24. Zhang B, Liu SH, Chi JH. Thermal hazard analysis and thermokinetic calculation of 1,3-dimethylimidazolium nitrate via TG and VSP2. J Therm Anal Calorim. 2018;134(3):2367–74.
25. Ozawa T. A new method of analyzing thermogravimetric data. Chem Soc Jpn. 1965;38:1881–6.
26. Feng WQ, Lu YH, Chen Y, Lu YW, Yang T. Thermal stability of imidazolium-based ionic liquids investigated by TG and FTIR techniques. J Therm Anal Calorim. 2016;125(1):143–54.
27. Starink MJ. A new method for the derivation of activation energies from experiments performed at constant heating rate. Thermochim Acta. 1996;288:97–104.
28. Kissinger HE. Reaction kinetics in differental thermal analysis. Anal Chem. 1957;29:1702–6.
29. Wei R, Huang S, Wang Z, Yuen R, Wang J. Evaluation of the critical safety temperature of nitrocellulose in different forms. J Loss Prev Process Ind. 2018;56:289–99.
30. Maton C, De Vos N, Stevens CV. Ionic liquid thermal stabilities: decomposition mechanisms and analysis tools. Chem Soc Rev. 2013;42(13):5963–77.
31. Cao Y, Mu T. Comprehensive Investigation on the Thermal Stability of 66 Ionic Liquids by Thermogravimetric Analysis. Ind Eng Chem Res. 2014;53(20):8651–64.
32. Liang R, Yang M, Xuan X. Thermal stability and thermal decomposition kinetics of 1-butyl-3-methylimidazolium dicyanamide. Chin J Chem Eng. 2010;18:736–41.
33. Lu GB, Yang T, Chen LP, Zhou YS, Chen WH. Thermal decomposition kinetics of 2-ethylhexyl nitrate under non-isothermal and isothermal conditions. J Therm Anal Calorim. 2016;124(1):471–8.
34. Lv JY, Chen WH, Chen LP. Thermal decomposition and isothermal kinetic model of bis-2, 4-dichlorobenzoyl peroxide. J Chem Ind Eng. 2013;11:4054–9.
35. Wang SY, Kossoy AA, Yao YD, Chen LP, Chen WH. Kinetics-based simulation approach to evaluate thermal hazards of benzaldehyde oxime by DSC tests. Thermochim Acta. 2017;655:319–25.
36. Zhang GY, Jin SH, Li LJ, Shu QH, Wang DQ, Zhang B, Li YK. Evaluation of thermal hazards and thermo-kinetic parameters of 3-amino-4-amidoximinofurazan by ARC and TG. J Therm Anal Calorim. 2016;126:1223–30.

37. Zhan ZJ, Chen XW, Lei M, Zhou YS, Zhang ZZ. Kinetics study of the synthesis of 1,3-diamino-1,2,3-trioximinopropane from the reaction of malononitrileoxime with hydroxylamine. Acta Chim Sin. 2011;69:1131–4.